Modeling Multivalent Ligand-Receptor Interactions with Steric Constraints on Configurations of Cell-Surface Receptor Aggregates

Michael I. Monine,[†] Richard G. Posner,[‡§] Paul B. Savage,[¶] James R. Faeder,[∥] and William S. Hlavacek[†††*]

[†]Theoretical Biology and Biophysics Group, Theoretical Division and Center for Nonlinear Studies, Los Alamos National Laboratory, Los Alamos, New Mexico; [‡]Computational Biology Division, Translational Genomics Research Institute, Phoenix, Arizona; [§]Department of Biological Sciences, Northern Arizona University, Flagstaff, Arizona; [¶]Department of Chemistry and Biochemistry, Brigham Young University, Provo, Utah; [∥]Department of Computational Biology, University of Pittsburgh School of Medicine, Pittsburgh, Pennsylvania; and [††]Department of Biology, University of New Mexico, Albuquerque, New Mexico

ABSTRACT   We use flow cytometry to characterize equilibrium binding of a fluorophore-labeled trivalent model antigen to bivalent IgE-FcεRI complexes on RBL cells. We find that flow cytometric measurements are consistent with an equilibrium model for ligand-receptor binding in which binding sites are assumed to be equivalent and ligand-induced receptor aggregates are assumed to be acyclic. However, this model predicts extensive receptor aggregation at antigen concentrations that yield strong cellular secretory responses, which is inconsistent with the expectation that large receptor aggregates should inhibit such responses. To investigate possible explanations for this discrepancy, we evaluate four rule-based models for interaction of a trivalent ligand with a bivalent cell-surface receptor that relax simplifying assumptions of the equilibrium model. These models are simulated using a rule-based kinetic Monte Carlo approach to investigate the kinetics of ligand-induced receptor aggregation and to study how the kinetics and equilibria of ligand-receptor interaction are affected by steric constraints on receptor aggregate configurations and by the formation of cyclic receptor aggregates. The results suggest that formation of linear chains of cyclic receptor dimers may be important for generating secretory signals. Steric effects that limit receptor aggregation and transient formation of small receptor aggregates may also be important.

INTRODUCTION

Antigen recognition by mast cells is mediated by antigen-specific IgE antibody bound to FcεRI (1), a multimeric cell-surface receptor that binds IgE in a 1:1 ratio with a high avidity and a long lifetime (2,3). Interaction of a multivalent antigen with IgE-FcεRI complexes results in clustering of FcεRI, which initiates an intracellular signaling cascade that leads to the rapid release of histamine and other mediators of allergic reactions stored in cytoplasmic granules as well as the synthesis and secretion of yet other mediators (4).

Various reagents have been used to induce clustering of FcεRI (or IgE-FcεRI), including chemically crosslinked oligomers of IgE (5,6), monoclonal IgE- and FcεRI-specific antibodies (7–10), haptenated carrier molecules (11,12), and chemically synthesized antigens with either two or three identical hapten groups recognized by monoclonal anti-hapten IgE (13–18). Studies with these reagents have revealed that signaling and cellular responses can depend strongly on the properties of FcεRI aggregates (19).

Antigen valence is one factor that can affect cellular responses to antigen-induced aggregation of IgE-FcεRI complexes (6,19). Posner et al. (16) reported the synthesis of a trivalent antigen that elicits a potent cellular secretory response. However, a structurally similar bivalent antigen was observed not to elicit detectable levels of secretion. In more recent work, Posner et al. (17) reported the synthesis

of fluorophore-labeled bivalent and trivalent antigens and demonstrated, as in the study of Posner et al. (16), that the trivalent antigens are potent secretogues, whereas their bivalent analogs fail to stimulate detectable cellular secretory responses. A variety of evidence suggests that bivalent antigens are poor secretogues because they tend to aggregate receptors in the form of cyclic dimers, which produce weak or even inhibitory signals, or to bind the two antigen-combining sites of a single IgE molecule in cases where the antigen is sufficiently flexible and large enough to span the distance between the two antigen-combining sites of an IgE antibody (15,19–22).

Here, to investigate clustering of IgE-FcεRI complexes induced by trivalent antigens, which evidently differs in a functionally significant way from the clustering induced by bivalent analogs, we use flow cytometry to monitor equilibrium binding of fluorophore-labeled antigen to IgE-FcεRI complexes on rat basophilic leukemia (RBL) cells. The antigen, which is referred to as compound 6a by Posner et al. (17), is a synthesized Alexa-488-labeled compound with flexible glycol linkers connecting three symmetrically arrayed hapten groups, allowing it to be recognized by monoclonal anti-hapten IgE. We attempt to explain the flow cytometric binding data in terms of various mathematical models for the interaction of a trivalent ligand with a bivalent cell-surface receptor.

One of the ligand-receptor interaction models that we consider is the equilibrium continuum model of Goldstein and Perelson (23), which accounts for all possible acyclic aggregates that can be formed through the interaction of

a ligand with three identical sites and a cell-surface receptor with two identical sites. The model predicts that a gel or superaggregate containing large numbers of receptors can form on the cell surface under certain circumstances.

Other models that we consider are kinetic models related to the Goldstein-Perelson model that track finite-sized populations of molecules. These models are formulated using a rule-based modeling approach (24), which enables us to relax assumptions of the Goldstein-Perelson model. With this approach, we can formulate models that account for the kinetics of ligand-receptor interaction, cyclic receptor aggregates, and steric constraints on the configurations of receptor aggregates, which we can expect to be especially important for large aggregates. The first kinetic model that we consider is the so-called trivalent ligand-bivalent receptor (TLBR) model (25) and, like the Goldstein-Perelson model, is based on the equivalent-site hypothesis (26). This hypothesis states that ligand-receptor interactions are essentially independent of the molecular context in which they take place. The two models, for the same equilibrium parameters, yield results that converge in the continuum limit. The remaining models, which will be referred to as Models I–III, are extensions of the TLBR model that account for cyclic receptor aggregates and/or steric constraints on aggregate configurations. Other types of steric constraints have been considered in earlier work (27–30). Here, we will only be concerned with constraints on the spatial arrangement of molecules within molecular complexes. Likewise, we will not consider spatial effects arising from diffusion.

The rule-based modeling approach is based on the idea of using graphs to represent molecules and graph-rewriting rules to represent molecular interactions (24,31,32). A rule can be viewed as an implicit definition of a class of reactions, a set of reactions all involving a common transformation. The rules of a model specification often imply a large-scale chemical reaction network, which is the case for all of the rule-based models that we consider here. In fact, the networks implied by the rules of the TLBR model and Models I–III are so large that simulation of these models using conventional methods is impossible (24,25). Recently, this problem has been overcome by the development of kinetic Monte Carlo methods specifically designed for rule-based models (25,33,34). Here, we show how the method of Yang et al. (25) can be used to account for geometric constraints on the formation of molecular complexes.

The results of our model-based analysis of ligand-receptor binding data suggest that factors that limit the size of ligand-induced receptor aggregates, perhaps only transiently, explain why compound 6a is a potent secretogue. It seems likely that this ligand induces linear chains of cyclic dimers; however, no definitive conclusions can be drawn at this time. We also delineate how various steric constraints on ligand-induced receptor aggregate configurations generally affect multivalent ligand-receptor binding and gelation, extending earlier studies of gels on cell membranes (23,35–37).

MODELS

We assume that a trivalent ligand interacts with a bivalent cell-surface receptor in a well-mixed system. The three binding sites of the ligand are assumed to be identical, as are the two binding sites of the receptor. Due to the multivalent nature of the ligand and receptor, the number of distinct ligand-induced receptor aggregates that can form is very large (23–25). Among the different possible structures of receptor aggregates are chains, trees, and cyclic aggregates (see Fig. S1 of the Supporting Material). We assume that the ligand is such that it cannot bind both sites of a receptor at the same time.

We will consider five different models for the system described above, two of which have been formulated in earlier work. These models are the equilibrium continuum model of Goldstein and Perelson (23) and a kinetic version of this model (known as the TLBR model (25)). Both models are based on the equivalent-site hypothesis (26). We introduce three kinetic models, which account for steric constraints on configurations of receptor aggregates: a model allowing for formation of linear chains of cyclic receptor dimers, which we will refer to as Model I; and two models in which aggregates form on a hexagonal lattice, which we will refer to as Models II and III, respectively. Models I–III describe the formation of planar receptor aggregates anchored to the cell surface. Model II includes only acyclic receptor aggregates, whereas Models I and III consider cycles of two and six receptors, respectively. Model II is a special case of Model III.

Goldstein-Perelson model

The Goldstein-Perelson model (23) is based on the assumption of thermal equilibrium. Interactions between ligands and receptors include only two types of associative binding reactions: binding of a site on a free ligand to a site on a cell-surface receptor, and crosslinking of two receptors by a ligand. These interactions are characterized by the following dimensionless parameters,

$$c = 3K_1 C_\infty^L, \tag{1}$$

$$\beta = K_2 C^R, \tag{2}$$

where the equilibrium association constant K_1 characterizes the binding of a ligand site in solution to a receptor site, the equilibrium crosslinking constant K_2 characterizes the binding of a tethered ligand site to a receptor site, C_∞^L is the concentration of free ligand in solution at equilibrium, and C^R is the total concentration of receptors. Note that a linear chain elongation reaction is assumed to be characterized by the same crosslinking constant K_2 as a reaction that forms a branch.

The Goldstein-Perelson model accounts for all possible receptor aggregates except cyclic aggregates. A key element

of this model is a partition function, which is a sum of the concentrations of all possible linear and branched aggregates. The partition function can be used to obtain expressions for C_∞^L and the fraction of free (unbound) receptors, x (see the Supporting Material).

The model predicts the fraction of receptors in a gel, f_g (a large cluster of receptors connected by ligand-receptor bonds), which is given by
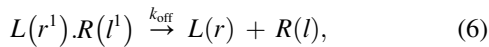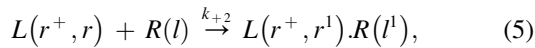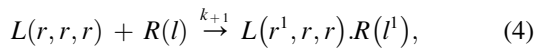
$$f_g = 1 - \frac{(1 + c)}{\beta}\left[1 + (1 + 1/c)^{1/2}\right]. \qquad (3)$$

Equation 3 with $f_g = 0$ describes the boundary of a percolation transition in the space of the parameters β and c. In the absence of a gel, the system contains free ligands, unaggregated cell-surface receptors, and small ligand-induced receptor aggregates.

TLBR model

The TLBR model is a kinetic version of the Goldstein-Perelson model formulated in terms of rules for ligand-receptor interactions (25). As indicated by the rules illustrated in Fig. 1, *a* and *b*, binding of a ligand from solution to a cell surface-receptor takes place with single-site forward rate constant k_{+1}, and crosslinking of receptors occurs with single-site rate constant k_{+2}. All association reactions are reversible, and dissociation occurs with single-site rate constant k_{off}.

The rules of the TLBR model can be specified using pseudo BioNetGen language (31) as

$$L(r,r,r) + R(l) \overset{k_{+1}}{\to} L(r^1,r,r).R(l^1), \qquad (4)$$

$$L(r^+,r) + R(l) \overset{k_{+2}}{\to} L(r^+,r^1).R(l^1), \qquad (5)$$

$$L(r^1).R(l^1) \overset{k_{off}}{\to} L(r) + R(l), \qquad (6)$$

where L denotes a ligand, R denotes a receptor, r denotes one of the three identical binding sites on a ligand, and l denotes one of the two identical binding sites on a receptor. The plus-symbol $(+)$ on the left-hand side of Eqs. 4 and 5 indicates that reacting sites must be members of distinct chemical species, i.e., a reaction implied by one of these rules has molecularity 2. The period (.) indicates that molecules are members of the same complex. The above rules represent capture of free ligand (Eq. 4), receptor crosslinking (Eq. 5), and ligand-receptor dissociation (Eq. 6). Reaction rate constants associated with these rules are single-site rate constants, k_{+1}, k_{+2}, and k_{off}, respectively. Note that the rule given by Eq. 5 states that a crosslinking reaction occurs if at least one site r on a ligand L is already bound to a receptor, which is indicated by the r^+ notation. The superscripts in Eqs. 4–6 indicate bonds; sites that share a common superscript are understood to be connected by a (noncovalent) bond.
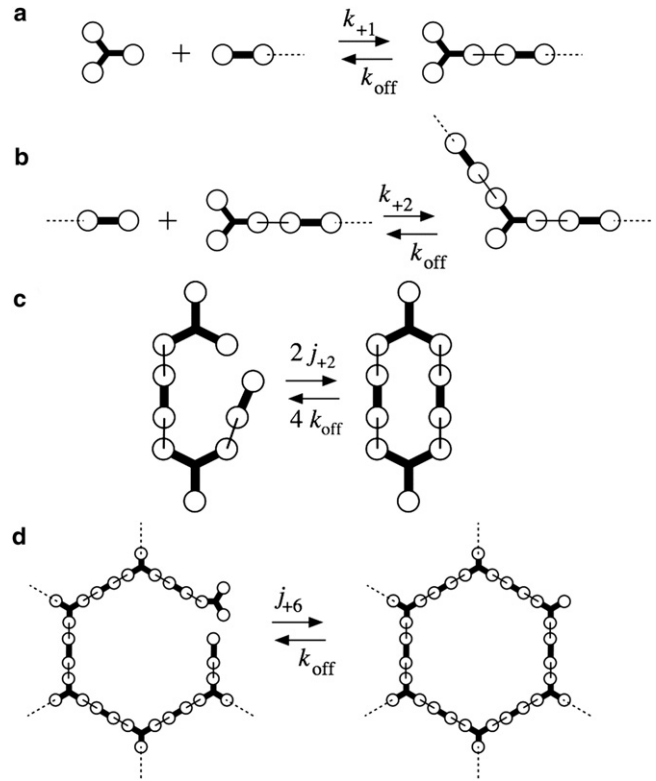
FIGURE 1 Reaction scheme of trivalent ligand-bivalent receptor interactions. Missing or variable parts of complexes are indicated by dotted lines. (*a*) A ligand from solution is captured by a cell-surface receptor with single-site rate constant k_{+1}. (*b*) A tethered ligand crosslinks two receptors with single-site rate constant k_{+2}. (*c*) Scheme of the dimer closure reaction. A factor of 2 before the single-site dimer closure rate constant j_{+2} indicates that there are two open ligand sites that a receptor can bind. Four bonds can break in a dissociation reaction. (*d*) In Model III, a hexagonal receptor aggregate can form with rate constant j_{+6} when free ligand and receptor sites belonging to the same aggregate are positioned next to each other. In all cases, dissociation is a context-independent reaction that occurs with single-site rate constant k_{off}.

Models with steric constraints

In the TLBR model, spatial configurations of receptors in aggregates are assumed to be unimportant. In contrast, in Models I–III, the rates of association reactions are assumed to depend on the configurations of receptors in aggregates.
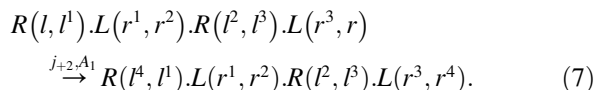
Models I–III involve rules with application conditions that specify constraints on receptor aggregate configurations. In Models I–III, all dissociation reactions, including ring-opening reactions, are characterized by a single-site rate constant, k_{off}. Ring closure reactions in Models I and III are characterized by single-site rate constants, j_{+2} and j_{+6}, respectively.

Model I

In Model I, we extend the TLBR model to include a ring-closure reaction. The formation of cycles is limited to cycles involving two receptors and two ligands with opposing ligand sites either free or occupied by receptors outside the cycle, as illustrated in Fig. 1 *c*. The single-site rate constant

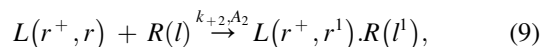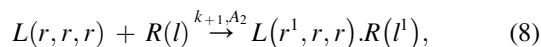for the ring-closure reaction is j_{+2}. The equilibrium ring-closure constant is $J_2 = j_{+2}/k_{off}$.

In addition to the three rules specified for the TLBR model (Eqs. 4–6), we introduce a new rule for the formation of a cyclic dimer, which we write as

$$R(l, l^1).L(r^1, r^2).R(l^2, l^3).L(r^3, r)$$
$$\overset{j_{+2}, A_1}{\rightarrow} R(l^4, l^1).L(r^1, r^2).R(l^2, l^3).L(r^3, r^4). \quad (7)$$

This rule indicates that formation of a cyclic structure is an intramolecular reaction, which occurs with single-site rate constant j_{+2}. The term A_1 indicates that an application condition must be satisfied before the rule can be applied. Here, A_1 is taken to mean that Eq. 7 applies only when a reaction results in a cyclic dimer. We exclude the formation of cyclic nonplanar aggregates with all ligand and receptor sites being occupied (38) as well as cycles that contain more than two receptors. A site of each ligand in a cyclic dimer can be free so that it can bind another receptor. As a result, larger aggregates can consist of linear chains of cyclic dimers, as shown in Fig. S6 a.
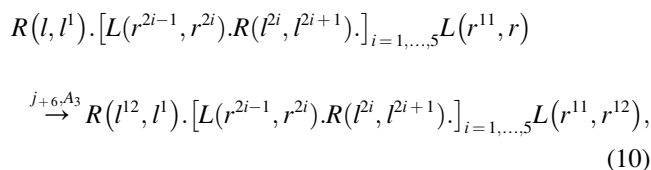
Model II

In Model II, we assume that ligands and receptors are rigid and we treat cell-surface reactions as if they occur on a hexagonal lattice, as shown in Fig. S1, b and c, and Fig. S4. To account for steric constraints on molecular structures of ligand-receptor aggregates, we track the connectivities and rotation angles of molecules in aggregates. Once a free ligand binds a surface receptor, the resulting complex only has freedom to rotate in two dimensions. Flips in three dimensions are not allowed. Two binding sites of different aggregates are not allowed to react if other parts of these aggregates overlap in space. In other words, steric clashes are prohibited. Model II is specified by Eq. 6 and the following rules, which are the same as Eqs. 4 and 5 except for a rule application condition,

$$L(r, r, r) + R(l) \overset{k_{+1}, A_2}{\rightarrow} L(r^1, r, r).R(l^1), \quad (8)$$

$$L(r^+, r) + R(l) \overset{k_{+2}, A_2}{\rightarrow} L(r^+, r^1).R(l^1), \quad (9)$$

where A_2 is meant to indicate that these rules do not apply when a reaction would result in a steric clash. The A_2 application condition is enforced by tree-traversal search of graphs representing aggregates to reject events that result in spatial overlaps.

Model III

Model III accounts for hexagonal cyclic structures. It is an extension of Model II. The only cyclic structure considered in Model III contains six receptors, and a single-site rate constant j_{+6} is used to characterize ring-closure reactions (Fig. 1 d). The rules for this model consists of Eqs. 6, 8, and 9 combined with the following rule for hexagonal ring closure,

$$R(l, l^1).\left[L(r^{2i-1}, r^{2i}).R(l^{2i}, l^{2i+1}).\right]_{i=1,\dots,5} L(r^{11}, r)$$

$$\overset{j_{+6}, A_3}{\rightarrow} R(l^{12}, l^1).\left[L(r^{2i-1}, r^{2i}).R(l^{2i}, l^{2i+1}).\right]_{i=1,\dots,5} L(r^{11}, r^{12}), \quad (10)$$

where A_3 is an application condition meant to indicate that the rule only applies for formation of cyclic structures containing six receptors. This application condition is enforced by a procedure that checks whether ligand and receptor sites are unbound and positioned next to each other in the same aggregate.

MATERIALS AND METHODS

Reagents

The ligand, a model antigen called compound 6a, was synthesized as described elsewhere (17). Compound 6a is composed of an Alexa-488 label and three symmetrically arrayed dinitrophenyl (DNP) groups. The maximum distance between two DNP groups is estimated to be ~50 Å based on Spartan-AM3 semiempirical calculations (17). This distance is significantly smaller than the distance between antigen-combining sites of IgE ($\approx$ 110–130 Å) (15,22).

The effective receptor consists of FcεRI expressed on RBL cells, tightly coupled to DNP-specific monoclonal IgE antibody from hybridoma H1 26.82 (39). The average lifetime of an IgE-FcεRI complex is >12 h (40), which is much longer than the timescale of a binding experiment. The mouse monoclonal anti-DNP IgE coupled to FcεRI on RBL cells was isolated from hybridoma H1 26.82 by affinity purification as described in Holowka and Metzger (41). Isolation of IgE involved, in the final steps, ion exchange chromatography, to remove bound DNP-glycine, and gel filtration, to separate monomeric IgE from IgE aggregates.

Cells

RBL-2H3 cells (42) were grown adherent in 75 cm^2 flasks. Cell cultures, which were used typically five days after passage, were maintained at 37°C. Culture media consisted of MEM $1\times$ with Earle's salts without glutamine (Gibco BRL, Gaithersburg, MD), 20% fetal bovine serum (HyClone, Logan, UT), 1% glutamine, 1% v/v penicillin, and 1% v/v streptomycin (Gibco BRL). To harvest cells, we rinsed and then incubated the cells, for 5 min at 37°C, with trypsin-EDTA. Cells harvested for experiments were washed and resuspended in buffered salt solution (pH 7.7), which was freshly passed through a 0.22-μm filter. Buffered salt solution consisted of 135 mM NaCl, 5 mM KCl, 1 mM MgCl$_2$ 1.8 mM CaCl$_2$, 5.6 mM glucose, 0.1% gelatin, and 20 mM HEPES. Cell suspensions in buffered salt solution were supplemented with 10 mM sodium azide and 10 mM 2-deoxy-glucose (Sigma, St. Louis, MO) to inhibit receptor recycling and cellular degranulation during binding experiments. To sensitize cells to DNP, we incubated cells overnight, while cells were still in culture, with excess (10 mg) anti-DNP IgE. Cells, which express FcεRI (at roughly 300,000 copies per cell (43)), were exposed to IgE for at least 12 h before harvesting.

Flow cytometric binding assays

Binding experiments were performed as described elsewhere (10). Briefly, we incubated a suspension of sensitized cells, with varying concentrations of Alexa-488-labeled ligand at room temperature. After incubating for at least 90 min, we used a FACScan flow cytometer (Becton Dickinson, Franklin Lakes, NJ), which was controlled with Cell Quest software, to collect histograms of fluorescence. Flow cytometric data were recorded as

the mean fluorescence (520 nm) of the cell suspension. To correct for nonspecific binding of ligand to cells, we performed a control experiment using cells lacking surface IgE and subtracted the mean fluorescence measured in this experiment from that measured in the corresponding experiment with sensitized cells.

Simulation of kinetic models

In the kinetic models, individual molecules and their sites are tracked explicitly. A detailed description of the data structures used for this purpose and the simulation algorithm are presented in the Supporting Material. The software used to simulate models is freely available upon request.

The TLBR model accounts for a set of three rule-defined reaction classes (Eqs. 4–6). These classes are ligand binding, receptor crosslinking, and dissociation. The reaction rules of Eqs. 4–6 are used in such a way that any reaction causes exchange of site addresses between lists of reactive sites. Reactive sites are identified based on the local context of interacting molecules in accordance with the method of Yang et al. (25). The procedure of next-reaction and reactive-site selection is described in the Supporting Material and by Yang et al. (25).

In the models with steric constraints, ligand binding from solution and receptor crosslinking are treated in the same way as in the TLBR model; however, final acceptance of reactions depends on a check of the spatial context of interacting molecules (see Step 2(e) of the simulation algorithm described in the Supporting Material). If a sampled reaction is not feasible for steric reasons, the reaction is rejected. To model ligand-receptor interactions on a hexagonal lattice, we use data structures that record the orientation angles of molecules and their binding sites (Models II and III), as described in the Supporting Material. To keep track of local configurations that participate in intramolecular reactions, we use data structures that record pairs of open ligand and receptor sites in acyclic dimers (Model I) and hexagonal open cells (Model III).

In contrast with the Goldstein-Perelson model, which is a continuum model, the kinetic models account for a finite-sized system. The size of the simulated system is defined by the total numbers of ligands, N_L, and receptors, N_R. The kinetic rate constants k_{+1} and k_{+2} are related to K_1 and K_2 as follows: $k_{+1} = K_1 k_{off}/(N_A V)$ and $k_{+2} = K_2 k_{off}/(N_A V)$, where V is the system volume and N_A is Avogadro's number. The relationships between k_{+1}, k_{+2} and the dimensionless parameters c and β of the continuum model are given as follows: $c = 3k_{+1}N_{L,\infty}/k_{off}$, and $\beta = k_{+2}N_R/k_{off}$, where $N_{L,\infty}$ denotes the number of free ligands in solution at equilibrium.

The efficiency of simulating the kinetic models depends on the system size, and therefore, to make simulations more tractable, we scale parameter values that are related to the system volume. We specify reference values for the volume (V^*) and the total numbers of receptors and ligands (N_R^* and N_L^*). The kinetic model parameters are scaled such that $V = \chi V^*$, $N_R = \chi N_R^*$, $N_L = \chi N_L^*$, $k_{+1} = \chi^{-1}k_{+1}^*$, and $k_{+2} = \chi^{-1}k_{+2}^*$, where χ is a volumetric scaling factor.

RESULTS

Analysis of equilibrium binding data

We used flow cytometry to monitor the association of Alexa-488-labeled ligand with cell-surface receptors at equilibrium as a function of ligand dose. We then fit the Goldstein-Perelson model to the binding data to determine best-fit parameter values. Fig. 2 a illustrates the agreement between the experimental data and the model fit. The best-fit values for K_1 and K_2 (and their 68% confidence intervals) are given in Table 1.

For best-fit parameter values, both the TLBR model and the Goldstein-Perelson model predict a sol-gel percolation transition (PT) and extensive receptor aggregation, or forma-
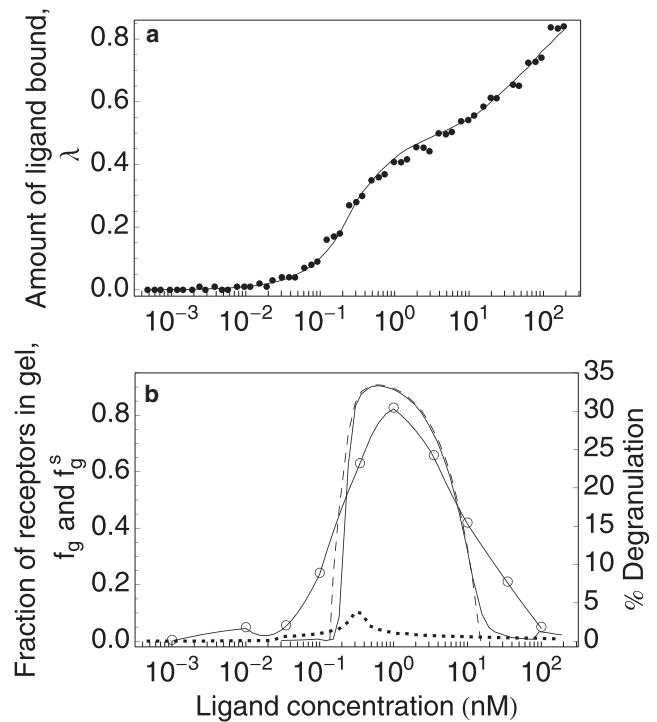
FIGURE 2 Fit of the Goldstein-Perelson or the TLBR model to flow cytometric binding data. (a) The y axis indicates the normalized amounts of ligand bound to cell-surface receptors, λ, at different ligand doses. Dots represent scaled measurements of average cell-associated fluorescence from the Alexa-488-labeled ligand. (b) Extensive aggregation is predicted by the TLBR model (solid line) and the Goldstein-Perelson model (dashed line) for ligand concentrations from 0.2 nM to 30 nM. The model with cyclic dimers, Model I (dotted line), predicts a sol phase at the same conditions. Parameter values used to calculate the aggregation curves are listed in Table 1. Other parameter values used in simulations of the kinetic models are $k_{off} = 0.01$ s^{-1}, $N_R^* = 300$, and volume $V^* = 10^{-12}$ L. Degranulation data from Posner et al. (17) are indicated by open dots.

tion of a gel phase, as ligand concentration increases from 0.2 nM to 30 nM, as shown in Fig. 2 b. The simulated fraction of receptors in the gel phase, f_g^s, agrees well with f_g, which is given by Eq. 3. Discrepancy between f_g^s and f_g can be attributed to finite-size effects (results not shown). These effects vanish as $\chi \to \infty$.

TABLE 1   Best-fit values for the equilibrium binding constants and scaling factor α for the Goldstein-Perelson and TLBR models and Model I, which accounts for cyclic dimers

| Parameters | Goldstein-Perelson and TLBR* models | | | Model I* |
	Estimate	Lower limit	Upper limit	Estimate
K_1 (nM^{-1})	0.467	0.111	0.767	6
K_2 (nM^{-1})	87.03	31.6	128.1	60
α	0.816	0.758	0.881	1

*Reference parameter values used in simulations are $V^* = 10^{-12}$ L (40), $N_{R^*} = 300$ molecules (43), $N_{L^*} = 4200$ molecules, $k_{off} = 0.01$ s^{-1} (11), and $J_2 = 5 \times 10^3$ (20). The values for V^*, N_{R^*}, and N_{L^*} are given for 0.1% of the volume of a cell and a cell density of 10^6 cells/mL. Confidence intervals are based on Fig. S2.

Fitting of the Goldstein-Perelson or TLBR model to the experimental data is described in the Supporting Material. Extensive receptor aggregation is predicted at ligand concentrations that yield strong secretory responses (Fig. 2 b). This finding contradicts studies indicating that extensive receptor aggregation inhibits secretory responses (4,44,45). We consider the following possible explanations for this discrepancy:

1. Large receptor aggregates are not inhibitory for the ligand used here and in Posner et al. (17);
2. Predictions of the Goldstein-Perelson or TLBR model cannot be trusted because this model is oversimplified (e.g., it does not account for cyclic aggregate formation or steric constraints on receptor aggregates); and
3. Large aggregates may be inhibitory, but these aggregates form late in the response to ligand and the early dynamics of receptor aggregation play a dominant role in triggering secretion.

To investigate hypotheses 2 and 3, we study the TLBR model and Models I–III.

Effect of cyclic receptor dimers

Unbound ligand and receptor sites of an open dimer, like that shown in Fig. 1 c, are allowed to interact with intramolecular rate constant j_{+2}, which has been chosen so that $J_2 = j_{+2}/k_{off} = 5000$, as in Posner et al. (20). In the resulting cyclic structure, the ligand/receptor ratio is 2:2.

We fit Model I, which accounts for cyclic dimers, to the equilibrium binding data in the same fashion as before. In the parameter space of K_1 and K_2, the region of best fit is shifted to higher values of $K_1 \approx 10^9$–10^{10} M^{-1} (results not shown). The quality of fit is comparable to that illustrated in Fig. 2. The best-fit values for K_1 and K_2 are given in Table 1 (column 5).

As shown in Fig. 2 b, at a ligand concentration that corresponds to extensive receptor aggregation according to the Goldstein-Perelson model, ≈ 0.3 nM, Model I predicts formation of relatively small clusters. The maximum value of f_g^s predicted by Model I is significantly reduced compared to that predicted by the Goldstein-Perelson or TLBR model.

Hexagonal lattice constraints

In contrast with the TLBR model, the model with hexagonal aggregate structures, but without cyclic aggregates ($j_{+6} = 0$) (i.e., Model II), predicts a gradual change of f_g^s as the crosslinking parameter β is increased, even as the volumetric scaling factor χ goes to infinity, as illustrated in Fig. 3 a. Receptor aggregation is generally suppressed. When steric constraints are taken into account, the fraction of receptors in the gel phase decreases significantly over the considered range of ligand concentrations (0.01–100 nM).

The possibility for ring-closure reactions ($j_{+6} > 0$) changes the percolation behavior. By including these reactions in
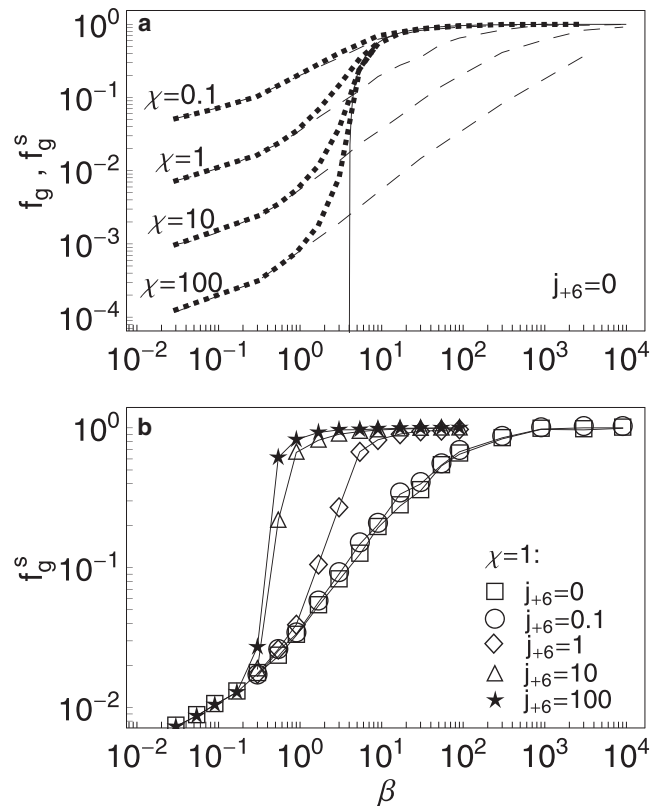

FIGURE 3 PT modified by finite-size effects and steric constraints. The y axis in each panel indicates the fraction of receptors in the gel phase. The x axis in each panel indicates the value of the dimensionless crosslinking rate constant β. (a) Finite-size effects in the TLBR model and Model II ($j_{+6} = 0$) depend on the volumetric scaling factor χ. Parameter values are scaled by χ as follows: $N_R = \chi N_R^*$, $N_L = \chi N_L^*$, $k_{+1} = \chi^{-1} k_{+1}^*$, and $k_{+2} = \chi^{-1} k_{+2}^*$. The value of f_g given by the Goldstein-Perelson model is indicated by the solid line. For $\chi = 0.1, 1, 10$, and 100, calculations based on the TLBR model (dotted lines) and Model II (dashed lines) are shown. The TLBR model approaches the continuum model as $\chi \rightarrow \infty$. (b) Effect of j_{+6} on the PT according to Model III. Increase of j_{+6} above 100 does not have a significant effect on the PT. In all calculations, we used the following parameter values: $N_R^* = 300$, $N_L^* = 4200$, $c = 0.36$ ($k_{+1}^* = 3 \times 10^{-7}$ molecules^{-1} s^{-1} and $N_{L,\infty} \approx N_L$), $k_{+2}^* = \beta k_{off}/N_R^*$ s^{-1}, and $k_{off} = 0.01$ s^{-1}.

Model III (which reduces to Model II when $j_{+6} = 0$), the effects of steric constraints are reversed. As shown in Fig. 3 b, an increase in the value of rate constant j_{+6} makes the PT steeper (i.e., more sensitive to the value of β). As $j_{+6} \rightarrow \infty$, the PT occurs at a much lower value of β compared to that in the TLBR model (~10 times lower), and the transition becomes steep. The approximate PT boundary simulated using Model III with $j_{+6} = 100$ s^{-1} is shown in Fig. S5 a. Formation of stable rings increases the size of the gel region in this phase plot because each hexagonal cycle in a receptor aggregate has up to six ligand sites free for receptor crosslinking.

Influence of the ring-closure rate constant, j_{+6}, on receptor aggregate structure is illustrated in Fig. 4. The fraction of receptors in the gel phase, f_g^s, as a function of j_{+6} at different system sizes (i.e., at different values of χ), is shown in Fig. 4 a. A critical range of j_{+6} values, in which the PT occurs,
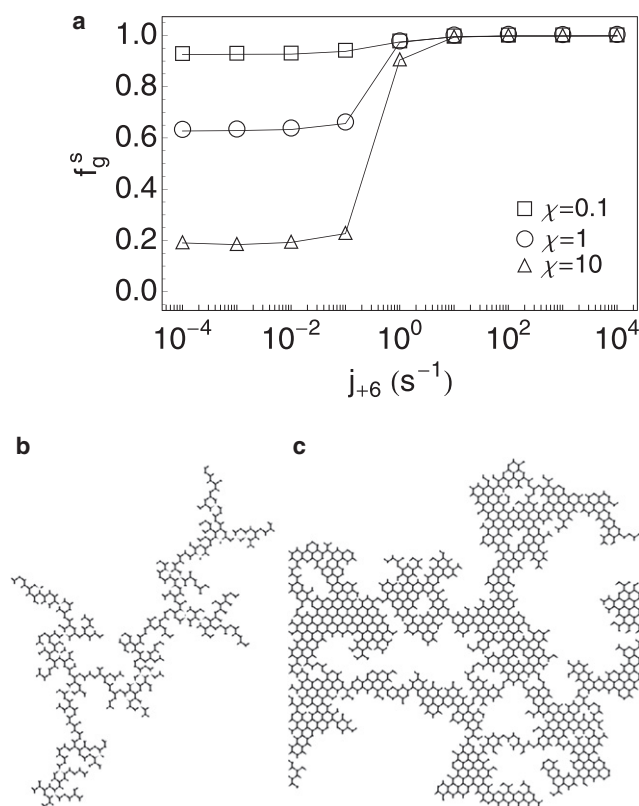
FIGURE 4   Effect of j_{+6} on cyclic receptor aggregates in Model III. (*a*) f_g^s is used as a measure of the aggregate density. At larger system volume (e.g., at $\chi = 10$ vs. $\chi = 0.1$), the difference in values of f_g^s whereas j_{+6} is varied is steeper because of finite-size effects. (*b* and *c*) Snapshots of simulations showing two fragments of aggregates: (*b*) a low-density structure (obtained with $j_{+6} = 0$), and (*c*) a high-density structure (obtained with $j_{+6} = 100$ s^{-1}). In all calculations, we used the following parameter values: $N_R^* = 300$, $N_L^* = 4200$, $c = 0.36$ ($k_{+1}^* = 3 \times 10^{-7}$ molecules^{-1} s^{-1}, $N_{L,\infty} \approx N_L$), $\beta = 90$ ($k_{+2}^* = 3 \times 10^{-3}$ s^{-1}), and $k_{off} = 0.01$ s^{-1}.

spans 0.1–1 s^{-1}. A decrease or increase of j_{+6} out of this range does not cause significant changes. For $j_{+6} < 0.1$, formation of open cycles (illustrated on the *left side* of Fig. 1 *d*) is the rate-limiting step in aggregation kinetics; for $j_{+6} > 1$, ring closure stabilizes open cycles once such aggregates form. Increase of the system size makes the transition of f_g^s more pronounced, but does not influence the range of sensitivity to j_{+6}. The value of f_g^s can also serve as a characteristic of the density of aggregates. Fig. 4 *b* shows a fragment of a branched aggregate predicted to form in one particular simulation of Model II ($j_{+6} = 0$, no ring closure). In contrast, for Model III with $j_{+6} = 10^4$ s^{-1}, cycles are stable and simulated aggregates have a denser structure characterized by $f_g^s \approx 1$, as shown in Fig. 4 *c*.

As shown in Fig. S7, hexagonal lattice constraints can be effectively captured using an empirical function that characterizes the dependence of binding probability, $P(s_l, s_r)$, on the sizes of associating aggregates, s_l and s_r, and lumped into factors that multiply binding rate constants.

Dynamics of aggregation

In our earlier work (25), we found that the TLBR model predicts that small receptor aggregates form transiently before the formation of a superaggregate. As seen from the simulation results of Fig. S8, similar dynamical behavior is predicted by Model II ($j_{+6} = 0$). Both the TLBR model and Model II also predict that two ligand doses (0.33 nM and 8.3 nM), stimulating receptor aggregation to the same extent at equilibrium ($f_g \approx 0.5$), can generate qualitatively distinct time courses of receptor aggregation. A feature of both models at high ligand concentration (8.3 nM) is an over-shoot in the average receptor aggregate size (Fig. S9). In contrast, in Model III with $j_{+6} >> 0$, the transient behavior changes. As shown in Fig. S9, the overshoot seen in the case of $j_{+6} = 0$ at high ligand dose disappears.

DISCUSSION

Recently, Yang et al. (25) developed a kinetic Monte Carlo method that can be used to study multivalent ligand-receptor interactions. Yang et al. (25) also formulated the TLBR model, a kinetic version of the equilibrium continuum model of Goldstein and Perelson (23). We have now extended this model to account for structural properties of the interacting molecules that place steric constraints on molecular aggregates. We carried out an extensive analysis of steric effects, considering effects on both equilibrium and kinetic behavior.

As part of our analysis, we analyzed equilibrium binding data characterizing the interaction of a trivalent antigen, compound 6a (17), with bivalent IgE-FcϵRI. To fit these data to a predictive model and estimate model parameters describing ligand capture from solution and receptor cross-linking, we first considered the Goldstein-Perelson model (23). The model fits the data well (Fig. 2). We found that, at the best-fit parameter values, the model predicts the formation of a gel phase for an interval of ligand doses that yield strong secretory responses (17) (Fig. 2 *b*). However, this model prediction contradicts the results of previous studies that indicate that large aggregates inhibit secretory responses (4,44,45). The Goldstein-Perelson model, although it fits the binding data well, is probably oversimplified. It treats sites as equivalent and does not account for cyclic aggregates or steric clashes that limit the formation of large aggregates (Figs. 2–4). It also does not account for the dynamics of receptor aggregation, which may be important.

We extended the TLBR model (a kinetic version of the Goldstein-Perelson model) to incorporate formation of cyclic receptor dimers to obtain Model I. This model accounts for a cyclic receptor dimer with two opposing ligand sites that could be occupied to generate linear chains of cyclic receptor dimers (as illustrated in Fig. S6). Simulation results for this model are shown in Fig. 2 *b*. For a fixed value of the ring closure constant, J_2, we adjusted the parameter values K_1 and K_2 such that a good fit to the equilibrium binding data

was obtained. As expected, the extent of receptor aggregation is significantly lower in Model I compared to the results obtained with the Goldstein-Perelson and TLBR models (Fig. 2 *b*). In fact, a superaggregate is no longer predicted. Bivalent antigens similar to compound 6a are believed to predominantly induce cyclic receptor dimers, but they do not generate secretory responses. In contrast, crosslinked cyclic receptor dimers do produce robust secretory responses (20,21). For these reasons, we believe compound 6a may induce linear chains of cyclic dimers, which prohibit super-aggregate formation.

To investigate steric effects due to excluded binding sites within ligand-induced receptor aggregates, we extended the TLBR model to track configurations of receptor aggregates explicitly. The resulting models, Models II and III, are based on the assumption that ligands and receptors are rigid and that receptor aggregates form on a hexagonal lattice. In making this assumption, we consider a case that can be viewed as opposite to that considered when making the assumption of equivalent sites. In the TLBR model, which is based on the equivalent-site hypothesis, there are no steric constraints on aggregate configurations at all, which corresponds to spacers between binding sites with infinite flexibility. For the ligand considered here (17), the spacers that connect the DNP groups are not rigid and a considerable amount of flexibility is possible. The spacers impose a maximum distance constraint and torsional preferences can be expected to favor maximum separation of the DNP groups. However, noncovalent interactions may bias the ligand toward other, more compact conformations. Note that the rigidity assumption is more valid for the trivalent ligands of Sil et al. (18), because the double-stranded DNA spacers that connect the DNP groups in these ligands are far more rigid.

Analysis of Model II, in which cyclic structures are not allowed, suggests that steric clashes of parts of interacting complexes limit aggregation significantly by excluding binding sites from interactions (Fig. 3 *a*). However, behavior of the model changes dramatically if cyclic aggregates are included (Fig. 3 *b*). In Model III, cyclic aggregates form on hexagonal cells. If the rings considered in Model III are stable ($j_{+6} >> 0$), they essentially turn individual bivalent receptors into six-valent receptors for ligand. In this case, ring-closure reactions lead to formation of stable aggregates of high receptor density (Fig. 4), quite unlike the behavior predicted by Model I, according to which the density of aggregates is reduced as a result of ring-closure reactions.

The dynamics predicted by the TLBR model and Model II are qualitatively similar (compare Fig. S8 of this work and Fig. 4 of Yang et al. (25)). We hypothesize that early formation of small aggregates may have a positive effect on secretion. Further growth in aggregate size and reduction in the number of small aggregates may then have a negative effect on secretion, consistent with earlier studies reporting inhibition of secretion by large receptor aggregates (4,44,45). In these models, at high rates of ligand capture from solution, the extent of aggregation passes through a maximum during the initial time course and then decreases to the equilibrium level (see Fig. S9). However, when rings are considered (i.e., Model II is extended to Model III) and $j_{+6} >> 0$, ring-closure reactions enhance receptor crosslinking and eliminate overshoot in receptor aggregation, even at high ligand doses (see Fig. S9).

It should be noted that steric constraints that affect the interaction of a free receptor site with a free site on a tethered ligand have been considered in earlier studies (15,27,28). These constraints, especially those considered by Schweitzer-Stenner et al. (15), affect the equilibrium crosslinking constant and can be accounted for implicitly: the less favorable the interaction, the smaller the crosslinking constant. Similar considerations may be useful for considering more realistic configurations of receptor aggregates.

The methodology developed here for studying steric constraints on receptor aggregate configurations can potentially be applied to an array of other problems where the geometric properties of interacting molecules constrain or facilitate interactions. The modeling approach may even be extended to account for the structures of interacting molecules in three-dimensional space.

SUPPORTING MATERIAL

REFERENCES

1. Kinet, J.-P. 1999. The high-affinity IgE receptor (FcϵRI): from physiology to pathology. *Annu. Rev. Immunol.* 17:931–972.

2. Kulczycki, Jr., A., and H. Metzger. 1974. The interaction of IgE with rat basophilic leukemia cells. II. Quantitative aspects of the binding reaction. *J. Exp. Med.* 140:1676–1695.

3. Garman, S. C., B. A. Wurzburg, …, T. S. Jardetzky. 2000. Structure of the Fc fragment of human IgE bound to its high-affinity receptor FcϵRIα. *Nature.* 406:259–266.

4. Metzger, H. 1992. Transmembrane signaling: the joy of aggregation. *J. Immunol.* 149:1477–1487.

5. Segal, D. M., J. D. Taurog, and H. Metzger. 1977. Dimeric immunoglobulin E serves as a unit signal for mast cell degranulation. *Proc. Natl. Acad. Sci. USA.* 74:2993–2997.

6. Fewtrell, C., and H. Metzger. 1980. Larger oligomers of IgE are more effective than dimers in stimulating rat basophilic leukemia cells. *J. Immunol.* 125:701–710.

7. Conrad, D. H., E. Studer, …, T. Mohanakumar. 1983. Properties of two monoclonal antibodies directed against the Fc and Fab′ regions of rat IgE. *Int. Arch. Allergy Appl. Immunol.* 70:352–360.

8. Menon, A. K., D. Holowka, …, B. Baird. 1986. Cross-linking of receptor-bound IgE to aggregates larger than dimers leads to rapid immobilization. *J. Cell Biol.* 102:541–550.

9. Ortega, E., R. Schweitzer-Stenner, and I. Pecht. 1988. Possible orientational constraints determine secretory signals induced by aggregation of IgE receptors on mast cells. *EMBO J.* 7:4101–4109.

10. Posner, R. G., J. M. Paar, …, W. S. Hlavacek. 2004. Interaction of a monoclonal IgE-specific antibody with cell-surface IgE-FcϵRI: characterization of equilibrium binding and secretory response. *Biochemistry.* 43:11352–11360.

11. Xu, K., B. Goldstein, …, B. Baird. 1998. Kinetics of multivalent antigen DNP-BSA binding to IgE-FcϵRI in relationship to the stimulated tyrosine phosphorylation of FcϵRI. *J. Immunol.* 160:3225–3235.

12. Hlavacek, W. S., A. S. Perelson, …, R. G. Posner. 1999. Quantifying aggregation of IgE-FcϵRI by multivalent antigen. *Biophys. J.* 76:2421–2431.

13. Erickson, J., P. Kane, …, B. Baird. 1986. Cross-linking of IgE-receptor complexes at the cell surface: a fluorescence method for studying the binding of monovalent and bivalent haptens to IgE. *Mol. Immunol.* 23:769–781.

14. Kane, P., J. Erickson, …, D. Holowka. 1986. Cross-linking of IgE-receptor complexes at the cell surface: synthesis and characterization of a long bivalent hapten that is capable of triggering mast cells and rat basophilic leukemia cells. *Mol. Immunol.* 23:783–790.

15. Schweitzer-Stenner, R., A. Licht, …, I. Pecht. 1987. Oligomerization and ring closure of immunoglobulin E class antibodies by divalent haptens. *Biochemistry.* 26:3602–3612.

16. Posner, R. G., P. B. Savage, …, W. S. Hlavacek. 2002. A quantitative approach for studying IgE-FcϵRI aggregation. *Mol. Immunol.* 38:1221–1228.

17. Posner, R. G., D. Geng, …, P. B. Savage. 2007. Trivalent antigens for degranulation of mast cells. *Org. Lett.* 9:3551–3554.

18. Sil, D., J. B. Lee, …, B. Baird. 2007. Trivalent ligands with rigid DNA spacers reveal structural requirements for IgE receptor signaling in RBL mast cells. *ACS Chem. Biol.* 2:674–684.

19. Holowka, D., D. Sil, …, B. Baird. 2007. Insights into immunoglobulin E receptor signaling from structurally defined ligands. *Immunol. Rev.* 217:269–279.

20. Posner, R. G., K. Subramanian, …, B. Baird. 1995. Simultaneous cross-linking by two nontriggering bivalent ligands causes synergistic signaling of IgE-FcϵRI complexes. *J. Immunol.* 155:3601–3609.

21. Harris, N. T., B. Goldstein, …, B. Baird. 1997. Altered patterns of tyrosine phosphorylation and Syk activation for sterically restricted cyclic dimers of IgE-FcϵRI. *Biochemistry.* 36:2237–2242.

22. Baird, E. J., D. Holowka, …, B. Baird. 2003. Highly effective poly(ethylene glycol) architectures for specific inhibition of immune receptor activation. *Biochemistry.* 42:12739–12748.

23. Goldstein, B., and A. S. Perelson. 1984. Equilibrium theory for the clustering of bivalent cell surface receptors by trivalent ligands. Application to histamine release from basophils. *Biophys. J.* 45:1109–1123.

24. Hlavacek, W. S., J. R. Faeder, …, W. Fontana. 2006. Rules for modeling signal-transduction systems. *Sci. STKE.* 2006:re6.

25. Yang, J., M. I. Monine, …, W. S. Hlavacek. 2008. Kinetic Monte Carlo method for rule-based modeling of biochemical networks. *Phys. Rev. E Stat. Nonlin. Soft Matter Phys.* 78:031910.

26. Perelson, A. S., and C. DeLisi. 1980. Receptor clustering on a cell surface. I. Theory of receptor cross-linking by ligands bearing two chemically identical functional groups. *Math. Biosci.* 48:71–110.

27. Dembo, M., and B. Goldstein. 1978. A thermodynamic model of binding of flexible bivalent haptens to antibody. *Immunochemistry.* 15:307–313.

28. DeLisi, C. 1980. The biophysics of ligand-receptor interactions. *Q. Rev. Biophys.* 13:201–230.

29. Schweitzer-Stenner, R., A. Licht, and I. Pecht. 1992. Dimerization kinetics of the IgE-class antibodies by divalent haptens. I. The Fab-hapten interactions. *Biophys. J.* 63:551–562.

30. Hlavacek, W. S., R. G. Posner, and A. S. Perelson. 1999. Steric effects on multivalent ligand-receptor binding: exclusion of ligand sites by bound cell surface receptors. *Biophys. J.* 76:3031–3043.

31. Faeder, J. R., M. L. Blinov, and W. S. Hlavacek. 2009. Rule-based modeling of biochemical systems with BioNetGen. *Methods Mol. Biol.* 500:113–167.

32. Feret, J., V. Danos, …, W. Fontana. 2009. Internal coarse-graining of molecular systems. *Proc. Natl. Acad. Sci. USA.* 106:6453–6458.

33. Danos, V., J. Feret, …, J. Krivine. 2007. Scalable simulation of cellular signaling networks. *Lect. Notes Comput. Sci.* 4807:139–157.

34. Colvin, J., M. I. Monine, …, R. G. Posner. 2009. Simulation of large-scale rule-based models. *Bioinformatics.* 25:910–917.

35. Guo, C., and H. Levine. 1999. A thermodynamic model for receptor clustering. *Biophys. J.* 77:2358–2365.

36. Barisas, B. G. 2003. Aggregation and gelation of divalent cell surface receptors by rigid polyvalent ligands: examination by theoretical, kinetic and thermodynamic techniques. *Thermochim. Acta.* 400:1–20.

37. Nag, A., M. I. Monine, …, B. Goldstein. 2009. Aggregation of membrane proteins by cytosolic cross-linkers: theory and simulation of the LAT-Grb2-SOS1 system. *Biophys. J.* 96:2604–2623.

38. Bilgiçer, B., D. T. Moustakas, and G. M. Whitesides. 2007. A synthetic trivalent hapten that aggregates anti-2,4-DNP IgG into bicyclic trimers. *J. Am. Chem. Soc.* 129:3722–3728.

39. Liu, F. T., J. W. Bohn, …, D. H. Katz. 1980. Monoclonal dinitrophenyl-specific murine IgE antibody: preparation, isolation, and characterization. *J. Immunol.* 124:2728–2737.

40. Faeder, J. R., W. S. Hlavacek, …, B. Goldstein. 2003. Investigation of early events in FcϵRI-mediated signaling using a detailed mathematical model. *J. Immunol.* 170:3769–3781.

41. Holowka, D., and H. Metzger. 1982. Further characterization of the β-component of the receptor for immunoglobulin E. *Mol. Immunol.* 19:219–227.

42. Barsumian, E. L., C. Isersky, …, R. P. Siraganian. 1981. IgE-induced histamine release from rat basophilic leukemia cell lines: isolation of releasing and nonreleasing clones. *Eur. J. Immunol.* 11:317–323.

43. Erickson, J., B. Goldstein, …, B. Baird. 1987. The effect of receptor density on the forward rate constant for binding of ligands to cell surface receptors. *Biophys. J.* 52:657–662.

44. Becker, K. E., T. Ishizaka, …, P. M. Grimley. 1973. Surface IgE on human basophils during histamine release. *J. Exp. Med.* 138:394–409.

45. Metzger, H. 2002. Molecular versatility of antibodies. *Immunol. Rev.* 185:186–205.